Anal. Chem. **2002,** *74,* 6314−6322

Poisson and Multinomial Mixture Models for Multivariate SIMS Image Segmentation

Alan Willse[†] and Bonnie Tyler*[,‡]

Departments of Mathematics, Montana State University-Bozeman, Bozeman, Montana 59717, and Department of Chemical and Fuels Engineering, University of Utah, 50 S. Central Campus Drive, Salt Lake City, Utah 84112-9203

Multivariate statistical methods have been advocated for analysis of spectral images, such as those obtained with imaging time-of-flight secondary ion mass spectrometry (TOF-SIMS). TOF-SIMS images using total secondary ion counts or secondary ion counts at individual masses often fail to reveal all salient chemical patterns on the surface. Multivariate methods simultaneously analyze peak intensities at all masses. We propose multivariate methods based on Poisson and multinomial mixture models to segment SIMS images into chemically homogeneous regions. The Poisson mixture model is derived from the assumption that secondary ion counts at any mass in a chemically homogeneous region vary according to the Poisson distribution. The multinomial model is derived as a standardized Poisson mixture model, which is analogous to standardizing the data by dividing by total secondary ion counts. The methods are adapted for contextual image segmentation, allowing for spatial correlation of neighboring pixels. The methods are applied to 52 mass units of a SIMS image with known chemical components. The spectral profile and relative prevalence for each chemical phase are obtained from estimates of model parameters.

Spectral imaging is one of the fastest growing areas of analytical chemistry and presents a variety of challenges for the analyst. In this paper, we have developed statistically based mixture models for identifying chemically unique regions in spectral images. These models are applied here to time-of-flight secondary ion mass spectrometry (TOF-SIMS) images but should be adaptable for use with a variety of spectral imaging techniques.

TOF-SIMS images over select mass ranges do not always reveal the chemical phases on the uppermost monolayer of a surface. Even if they could, the analyst may be unsure which mass ranges to select for imaging, especially if the surface chemistry is unknown. Examination of an entire "fingerprint" region of the spectra, including relative peak intensities, may be required to distinguish different chemical phases on the surface. Multivariate statistical methods, which simultaneously consider all peak intensities, have been successfully applied to SIMS images to reveal distinct chemical patterns.[1−3]

Of the multivariate methods, principal components analysis is used frequently in SIMS applications.[1] More recently, neural networks have been adapted to cluster SIMS images into chemically homogeneous regions.[2,3] Mixture models have become popular tools for image segmentation,[4] but they have never been adapted for analysis of SIMS images. Mixture model imaging applications almost always assume underlying multivariate normal distributions. In this paper we adapt the mixture model approach to SIMS images by modeling the secondary ion count data with Poisson and multinomial count distributions. Poisson and multinomial assumptions are often appropriate with low count data. In SIMS imaging of the uppermost monolayer, low count data are common when high lateral resolution is required. In other statistical applications with low count data, models based on Poisson and multinomial distributions have been shown to more powerfully reveal patterns in the data than methods based on approximating normal distributions.[5] Thus, the methods developed here may be most useful in the analysis of low count data.

Images are statistically analyzed for a variety of reasons, including enhancement, restoration, segmentation, and pattern recognition.[6] In this paper, we restrict our attention to segmentation of images into chemically homogeneous regions: the so-called image segmentation problem. We assume that each pixel is a member of a unique chemical class, but that the chemical classes are unknown. Profiles of the chemical classes must be gleaned from the observed spectra, and pixels must be assigned to chemical classes according to how well their spectra match the profiles. We do not consider the case of "mixed" pixels, in which one pixel may be composed of a mixture of two or more chemical classes, although mixture models can be extended, or fuzzified, to handle the mixed pixel problem.[7]

Unlike other methods proposed for SIMS imaging, the methods developed in this paper are derived from probability models. Methods based on probability models make statistical inference

* To whom correspondence should be addressed. Phone: (801)-587-9696. Fax: (801)-585-9291. E-mail: bonniet@eng.utah.edu.

[†] Montana State University-Bozeman.

[‡] University of Utah.

(1) Kargacin, M. E.; Kowalski, B. R. *Anal. Chem.* **1986**, *58*, 2300−2306.
(2) Wolkenstein, M.; Hutter, H.; Mittermayr, C.; Schiesser, W.; Grasserbauer, M. *Anal. Chem.* **1997**, *69*, 777−782.
(3) Olson, J. E.; Ingram, J. C.; Oroenwold, A. K.; Gianotto, A. K. In *Secondary Ion Mass Spectrometry: SIMS XI*; Gillen, G., Lareau, R., Bennett, J., Stevie, K., Eds.; Wiley: New York, 1998.
(4) McLachIan, G. J. Discriminant Analysis and Statistical Pattern Recognition; Wiley: New York, 1992; Chapter 13.
(5) McCuliagh, P.; Nelder, J. A. *Generalized Linear Models*, 2nd ed.; Chapman & Hall: London, 1989; Chapter 6.
(6) Pedersen, F.; Bengtsson, E.; Nordin, B. *J. Chemomem.* **1995**, *9*, 389−409.
(7) Caillol, H.; Pieczynski, W.; Hillion, A. *IEEE Trans. Image Proc.* **1997**, *6*, 425−440.

10.1021/ac025561i CCC: $22.00
Published on Web 11/08/2002

possible. Examples of statistical inference include estimation of standard errors, detection of outliers, and comparisons of different models. In addition, methods based on probability models may aid our understanding of the data-generation mechanism (which may contribute to theoretical developments). For example, by comparing several different probability models (data-generation mechanisms) for a data set, we may find that one model is more consistent with the data than the other models; that model might be considered an approximation to the data-generation mechanism.

The methods in this paper are extended to contextual image segmentation, in which neighboring pixels are allowed to be correlated. Noncontextual methods, in contrast, do not allow for correlated pixels. Previous SIMS image analysis applications considered only noncontextual methods.

THEORY

In SIMS imaging, secondary ion intensity spectra are collected at each pixel. Let $x_h = (x_{ih}, ..., x_{ph})$ denote peak counts for the hth pixel, so that x_h is the count at mass i for pixel h. We assume that each pixel can be classified into one of K distinct chemical classes. If $g_j(x_h, \Psi_j)$ is the density of peak counts for pixels in the jth chemical class, then the overall probability density function for a randomly chosen pixel of unknown chemical class is

$$f(x_h; \Psi) = \sum_{j=1}^{K} \eta_j g_j(x_h; \Psi_j) \qquad (1)$$

where η_j ($0 < \eta_j < 1; \sum_{j=1}^{K} \eta_j = 1$) represents the proportion of pixels at the jth chemical class. The η_j are also called prior class probabilities. The vector Ψ contains all unknown parameters. The density (eq 1) is called a finite mixture model in the statistics literature.[8] Finite mixture models are used to unmix, or segment, heterogeneous observations into separate homogeneous classes.

Poisson Model. Before finite mixture models can be applied in practice, a decision must be made about the functional forms of the class densities, $g_j(x_h, \Psi_j)$. Because the peak intensities are actually ion counts, it is natural to consider the Poisson distribution for the marginal density of the x_{ih}'s. The Poisson assumption can be approximately derived from consideration of the sputtering process.[9] In the acquisition of a SIMS image, each pixel receives N independent pulses from the primary ion beam, where N is generally large. For species i, the number of secondary ions detected from the rth pulse is distributed as binomial (n_r, p_i), where n_r is the total number of molecules that leave the surface on pulse r, and p_i is the probability that a molecule leaving the surface is detected as a secondary ion of species i. The total number of secondary ion species i detected over all N pulses is distributed as binomial.[10]

Because N is large and p_i is small, the distribution is well-approximated by a Poisson distribution[10] (this is true even if the observed counts are low). When ion counts are high, the Poisson distribution is adequately approximated by the normal distribution, but when counts are low, the Poisson distribution more accurately represents the data; it is here that the Poisson models may provide advantages over other methods. Low-count data are common in monolayer images with high lateral resolution.

Not enough is known about the ionization mechanism to determine whether noise (or statistical variation) is independent for different peaks in the same chemical class, but preliminary data analysis suggests that the assumption is plausible. We therefore assume that counts at different masses in a chemical phase are independent Poisson random variables. If a more complex correlation structure is suspected, it could be incorporated into the model. For comparison with other methods, we note that pattern recognition methods that use Euclidian distance as a measure of proximity (such as k-means cluster analysis and Kohonen networks) implicitly assume that variables within a class are independent and that they have the same marginal variances.

The mixture model for class-independent Poisson random variables is given by

$$f(x_h; \Psi) = \sum_{j=1}^{K} \eta_j \prod_{i=1}^{p} \frac{e^{-\lambda_{ij}} \lambda_{ij}^{x_i}}{x_i!} \qquad (2)$$

The Poisson parameters (λ_{1j}, ..., λ_{pj}) represent the pure spectra for the jth chemical class. For a sample of n independent observations, x_1, ... x_n, the joint sample probability density function is

$$f(x_1, L, x_n; \Psi) = \prod_{h=1}^{n} \left[\sum_{j=1}^{K} \eta_j \prod_{i=1}^{p} \frac{e^{-\lambda_{ij}} \lambda_{ij}^{x_{ih}}}{x_{ih}!} \right] \qquad (3)$$

The unknown parameters $\{\eta_j\}$ and $\{\lambda_{ij}\}$ and their asymptotic standard errors can be estimated by the method of maximum likelihood using the EM algorithm,[11] as described in the estimation section. For images with many pixels, the parameters can be adequately estimated from a random selection of the pixels. That saves computer time and also lends credibility to the assumption of independent observations (in general, we expect neighboring pixels to be correlated, as discussed below).

For classification, the hth pixel is allocated to the class with the largest posterior probability,

$$h(j|x_h, \Psi) = \frac{\eta_j \prod_{i=1}^{p} e^{-\lambda_{ij}} \lambda_{ij}^{x_{ih}}}{\sum_{l=1}^{K} \eta_l \prod_{i=1}^{p} e^{-\lambda_{ij}} \lambda_{ij}^{x_{ih}}} \qquad (4)$$

which is the probability that a pixel with observed spectrum x_h is from class j. In practice, parameter estimates are substituted in (4).

(8) Titterington, D. M.; Smith, A. K.; Makov, U. E. *Statistical Analysis of Finite Mixture Distributions*; Wiley: Chichester, 1985.

(9) Schwieters, J.; Cramer, H. O.; Helier, T.; Jurgens, E.; Niehuis, J.; Zehnpfenning, J.; Benninghoven, A. *J. Vac. Sci. Technol. A* **1991**, *9*, 2864−2871.

(10) Feller, W. *An Introduction to Probability Theory and its Applications*; Wiley: New York, 1968.

(11) McLachIan, O. J.; Krishnan, T. *The EM Algorithm and Extensions*; Wiley: New York, 1997.

An estimate of pixel misclassification rate is

$$\hat{err} = \frac{1}{n}\sum(1 - \max_j h(j|x_h, \hat{\Psi})) \quad (5)$$

If the posterior probabilities are all close to 0 or 1, the misclassification rates will be low.

To this point, we have assumed that the number of chemical classes, K, is known. In practice, K is usually unknown, and should be considered a parameter in the model. No segmentation method provides a perfectly satisfactory way to estimate K. Most methods rely on heuristics as guides to the choice of K. We use a statistically derived heuristic called Bayesian information criterion[12] (BIC), which is computed as

$$\text{BIC} = -2\log(L) + (\text{number of free parameters})\log(n) \quad (6)$$

where L is the maximized value of the log-likelihood function, $\log f(x_1, ..., x_n; \Psi)$. For the Poisson model, the number of free parameters is $K - 1 + pK$. The mixture model is fit for several choices of K, and the model giving the smallest BIC is selected as the "best" model. The process is interactive; the analyst should examine images and parameter estimates for different choices of K to assist in the decision.

In images, neighboring pixels tend to be correlated. That is, a pixel is a priori more likely to belong to a class that its neighbors belong to than to other classes. The development above, which did not account for this correlation, is called noncontextual image segmentation. Contextual image segmentation, in contrast, accounts for the correlation by modeling prior class probabilities for a pixel as a function of class assignments for its neighbors.[4] If η_{jh} is the prior probability that the hth pixel is a member of class j, then we assume

$$\eta_{jh} \propto \exp(\beta u_{jh}) \quad (7)$$

where u_{jh} is the number of neighbors of pixel h that belong to class j (in the noncontextual development, the subscript h was omitted from η_{jh} because prior class probabilities were assumed to be the same for all pixels). We take the neighborhood of pixel h to consist of the four adjacent pixels and the four diagonally adjacent pixels, where available. The parameter β is a measure of the strength of correlation between neighboring pixels. Because true classifications are unknown, the contextual image is estimated through an iterative process, called the ICM algorithm, which is described in the estimation section. The contextual image is estimated from the entire image data set, not just a random selection of pixels, so computation time will increase. Computation can be reduced if the parameters $\{\eta_{ij}\}$ and $\{\lambda_{ij}\}$ are estimated from a random selection of pixels and either assumed to be known or used as initial estimates in the contextual image estimation. The correlation parameter, β, can be estimated by numerical methods, but we choose to specify it a priori to save computation time. In practice, for most images, its value has been found to be between 0.7 and 1.5.[4] The practical effect of contextual analysis is to smooth the image. For this reason, the parameter β is sometimes called a smoothing parameter.

Multinomial Model. Topographic differences over the area analyzed may lead to excessive variation in counts for pixels from the same chemical class. For example, more secondary ions may be emitted and detected at surface peaks than at surface valleys. This may lead to estimation of too many chemical phases and may confound chemical variation with topographic variation. When this happens, it is useful to standardize the data by, for example, dividing each count by the total ion counts for the pixel. Under the assumption of independent Poisson random variables for a chemical class, an alternative form of standardization is to condition on total ion counts. This gives the mixture model

$$f(x|\sum_{i=1}^{p} x_i = y) = \sum_{j=1}^{K} \eta_{j|y} g_j(x|y) \quad (8)$$

where $\eta_{j|y}$ is the prior probability (that is, prior to observing x) of a pixel belonging to class j given total ion count y. In the absence of a priori evidence about the relationship between class probabilities and total ion counts (which is influenced by class membership and topography), it is reasonable to take $\eta_{j|y} = \eta_j$, which we do. Under the Poisson assumption for $g_j(x)$,

$$g_j(x|y) = \frac{y!}{x_1!x_2!\text{L}x_p!}\prod_{i=1}^{p}\pi_{ij}^{x_i} \quad (9)$$

which is the multinomial probability density function,[5] where $(\pi_{1j}, ..., \pi_{pj})$ represents the standardized pure spectrum for the jth chemical class. The multinomial mixture model is

$$f(x|\sum_{i=1}^{p} x_i = y) = \sum_{j=1}^{K} \eta_j \frac{y!}{x_1!x_2!\text{L}x_p!}\prod_{i=1}^{p}\pi_{ij}^{x_i} \quad (10)$$

Because the multinomial model conditions on total ion counts, some spectral information is lost. This may result in less separated chemical phases (especially in cases in which total ion counts adequately separate chemical phases) and a noisier image. However, the image, although noisy, will correct for topographical variation (we are assuming that topography influences ion counts). Parameter estimation via the EM algorithm is described in the estimation section. The model selection process is the same as that for the Poisson model. The number of free parameters in the multinomial model is K_{p-1}. Because the data are standardized, we would expect as many as or fewer classes with the multinomial model than with the Poisson model. Contextual multinomial images are created similarly to contextual Poisson images.

ESTIMATION

Noncontextual Analysis. Maximum likelihood estimates of the mixture model parameters can be obtained by treating the unobserved class labels as missing data and using the EM algorithm.[11] Let $z_h = (z_{1h}, ..., z_{kj})$ be the K-dimensional class

(12) Schwarz, O. *Ann. Stat.* **1978**, *6*, 461−464.

indicator vector for the hth pixel, so that $z_{jh} = 1$ if pixel h is from chemical class j, and $z_{jh} = 0$ otherwise. The z_h are not observed. The EM algorithm requires the complete-data log likelihood (over the observed data and the unobserved z_h), which is given by

$$L_c = \sum_{h=1}^{n}\sum_{j=1}^{K} z_{jh}\{\log \eta_j + \log g_j(x_h; \Psi)\} \tag{11}$$

where $g_i(x_h, \Psi)$ depends on the class-conditional probability assumption.

The EM algorithm is a two-step iterative procedure. In the E step (or expectation step) we compute

$$Q = E_z^{\Psi}(L_c) \tag{12}$$

where the expectation is taken with respect to the conditional distribution of the unobserved data z_h ($h = 1, ..., n$) given observed data and current parameter estimates $\hat{\Psi}$. Because L_c is linear in the unobserved data, the expectation is easily obtained by replacing each z_{jh} with $\hat{z}_{jh} = h(j|x_h, \hat{\Psi})$, where

$$h(j|x_h, \hat{\Psi}) = \frac{\eta_j g_j(x_h; \hat{\Psi}_j)}{\sum_{l=1}^{K} \eta_l g_l(x_h; \hat{\Psi}_l)} \tag{13}$$

is the posterior probability that pixel h is from class j.

In the M step (or maximization step), Q is maximized subject to the constraint $\sum_{j=1}^{K} \eta_j = 1$. This yields

$$\hat{\eta}_j = \frac{1}{n}\sum_{h=1}^{n} \hat{z}_{jh} \tag{14}$$

For the Poisson model (eq 2),

$$\hat{\lambda}_{ij} = \frac{1}{n\hat{\eta}_j}\sum_{h=1}^{n} \hat{z}_{jh} x_{ih} \tag{15}$$

and for the multinomial model (eq 10),

$$\hat{\pi}_{ij} = \frac{\sum_{h=1}^{n} \hat{z}_{jh} x_{ih}}{\sum_{h=1}^{n} \hat{z}_{jh} y_h} \tag{16}$$

where $y_h = \sum_{i=1}^{p} x_{ih}$.

The EM algorithm alternately updates eq 13 (E step) and eqs 14−16 (M step). The procedure requires starting values for the iterations. Starting values can be obtained by randomly initializing posterior probabilities $h(j|x_h, \Psi)$ uniformly on (0, 1) and then standardizing the uniform variates to satisfy $\sum_{j=1}^{K} h(j|x_h, \Psi) = 1$ for all h.

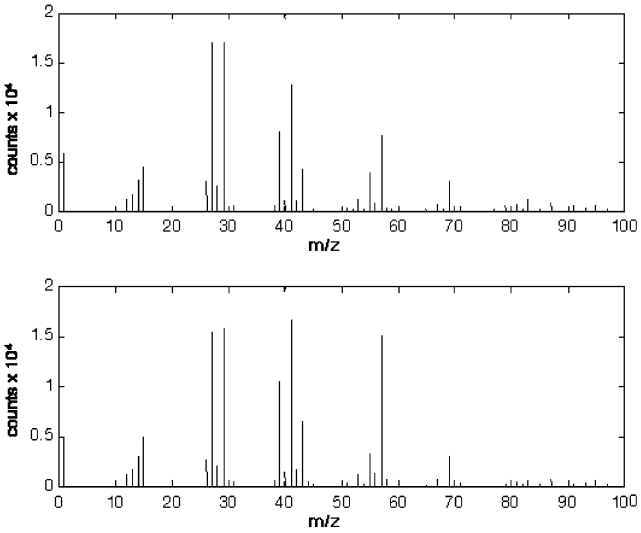

Figure 1. TOF-SIMS spectra of poly(*n*-butyl-methacrylate) (PNBMA) (top) and poly(isobutyl-methacrylate) (PIBMA) (bottom) collected with the Phi Trift I using a 25 kV gallium ion source.

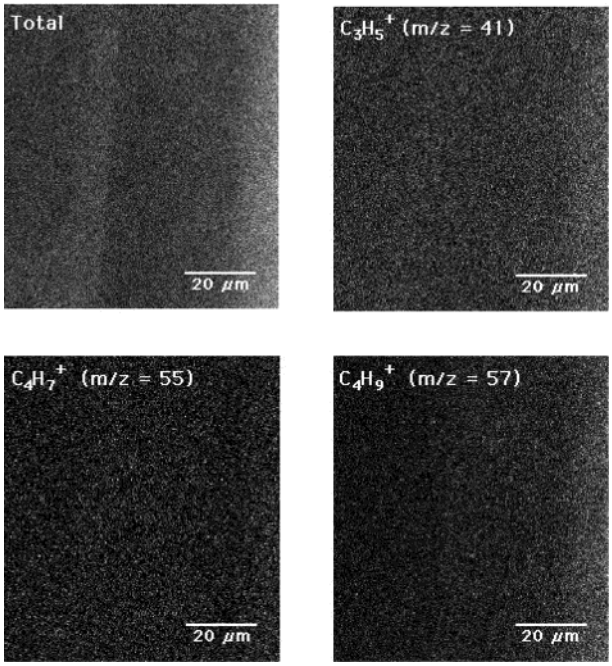

Figure 2. Selected ion images from a TOF-SIMS analysis of a PNBMA/PIBMA composite film on a silicon wafer. The images reveal topographic features but do not clearly reveal the two different polymer regions.

Approximate asymptotic~standard errors are given by the square roots of the diagonal elements of the matrix

$$\left(\sum_{h=1}^{n} \frac{1}{f(x_h; \hat{\Psi})^2} \frac{\partial f(x_h; \hat{\Psi})}{\partial \Psi} \frac{\partial f(x_h; \hat{\Psi})}{\partial \Psi'}\right)^{-1} \tag{17}$$

Details of the computation are omitted.

Contextual Analysis. When the class indicator vectors z_h are assumed to be correlated, the E step of the EM algorithm becomes complicated and an iterative estimation procedure known as the ICM algorithm is often preferred. The ICM algorithm was developed specifically for contextual image segmentation.[4]

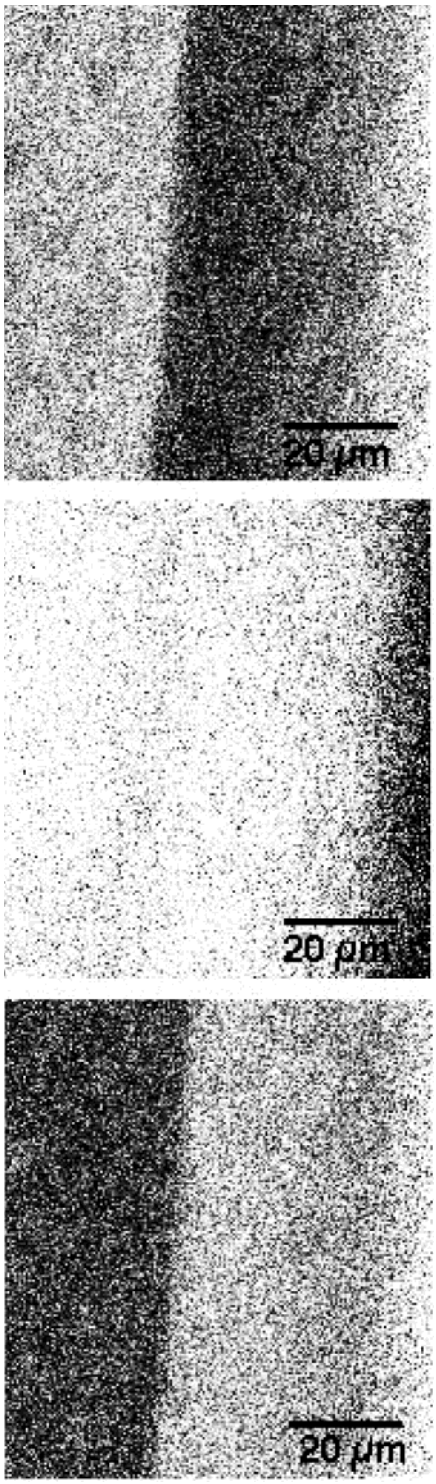

Figure 3. Images of the PNBMA/PIBMA film where the gray scale corresponds to the posterior probability that each pixel belongs to the component, on the basis of the 3 component Poisson model. Black indicates a probability of 1, and white, a probability of 0. The top image shows the posterior probabilities for component 1. Component 2 is displayed in the middle image, and component 3 is shown at the bottom.

If the correlation structure is given by eq 7, and if the smoothing parameter P and the model parameters are assumed to be known (adequate estimates of the model parameters can usually be obtained from a noncontextual analysis of a random sample of pixels), then the ICM algorithm assigns the hth pixel

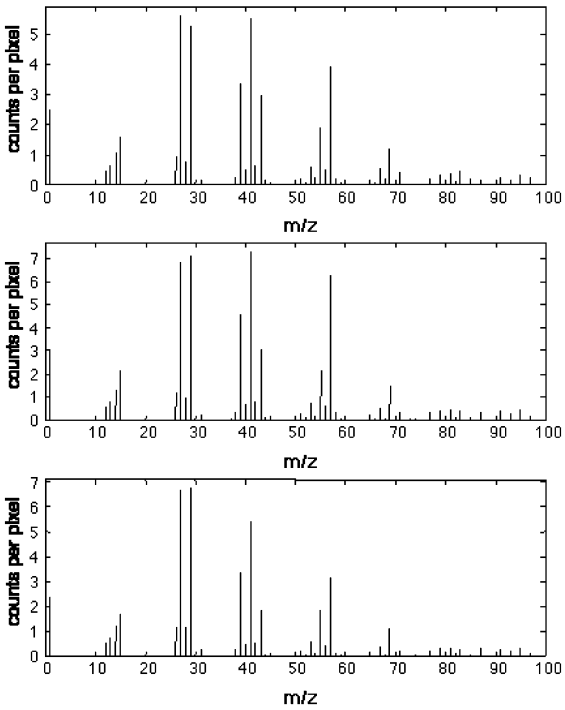

Figure 4. The latent profiles extracted from the PNBMA/PIBMA image using a 3-component Poisson model. The profile for component 1 (corresponding to the black pixels in Figure 5) is shown at the top, component 2 (Figure 5, gray) is shown in the middle, and component 3 (Figure 5, white) is displayed at the bottom.

(i.e., updates z_h) to the class j such that

$$g_j(x_h; \Psi_j) \exp(\beta u_{jh})$$

is a maximum. The process is applied to all pixels several times. If the model parameters are not assumed to be known, then their estimates can be updated within the ICM algorithm using 14−16, with the $\hat{z}_{jh}$ replaced by current ICM estimates of class assignments. The smoothing parameter β can also be estimated using the ICM algorithm, but in this paper, we assume β is known.

EXPERIMENTAL SECTION

Sample Description and Data Acquisition. A sample was prepared by spin-casting poly (*n*-butyl methacrylate) on a silicon wafer and then dipping one side of the sample in poly(isobutyl methacrylate). A 256 × 256 TOF-SIMS positive ion image of the sample was created using a Phi/Evans Trift I spectrometer equipped with a 25 kV Ga^+ primary ion source. The area of the sample scanned was 80 × 80 μm, and the lateral resolution was ∼300 nm. Spectral intensities were binned in 1-amu units. One amu binning was utilized because the image was collected using an unbunched 25 keV Ga^+ source, which did not permit high mass resolution. One amu binning is not necessary for use of the mixture model, which can easily accommodate high mass resolution data. Fifty-two peaks, from mass 1 to mass 97, were included in the analysis. This included all of the peaks present with an intensity of over 500 counts in the total image spectra. Larger masses can be easily included in the mixture model, but they were not present in this image. Although the total

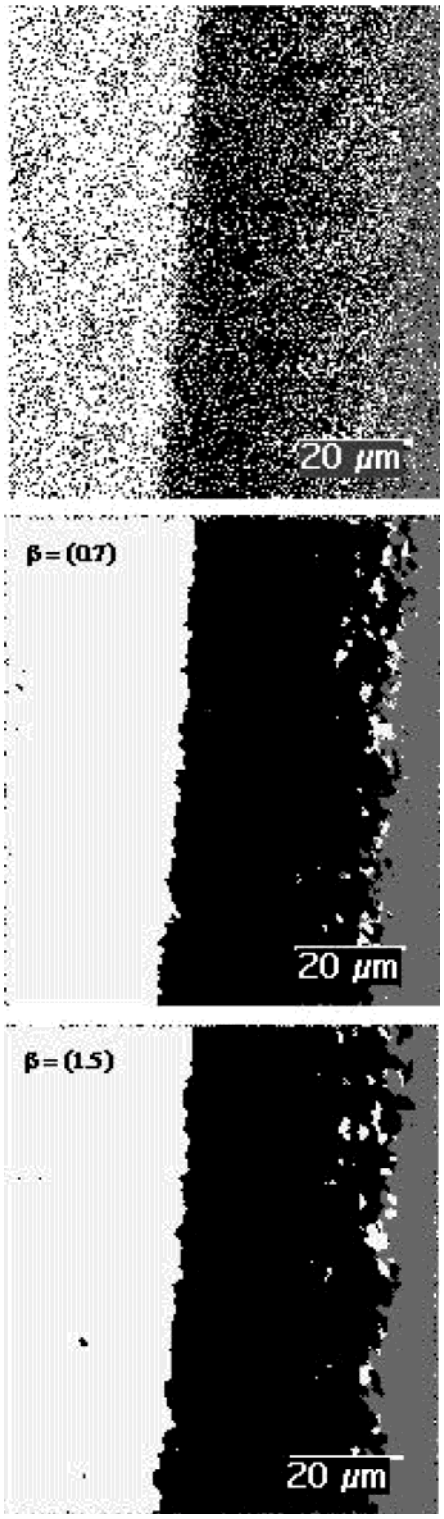

Figure 5. Images generated from the Poisson model by classifying each pixel into one of 3 classes. The top image shows classification using a smoothing parameter $\beta = 0$ (i.e., no contextual refinement). Contextual information was included to classify the pixels in the middle image ($\beta = 0.7$) and the bottom image ($\beta = 1.5$). In all of the images, pixels assigned to component 1 are shown in black, those assigned to component 2 are shown in gray, and those assigned to component 3 are shown in white.

intensity of all of the ions in the image exceeded 3×10^6 counts, the average per pixel ion intensity for the 52 peaks was <1 count, and the maximum ion intensity for any peak in any pixel was 21 counts. This low per-pixel signal is typical for static SIMS images.

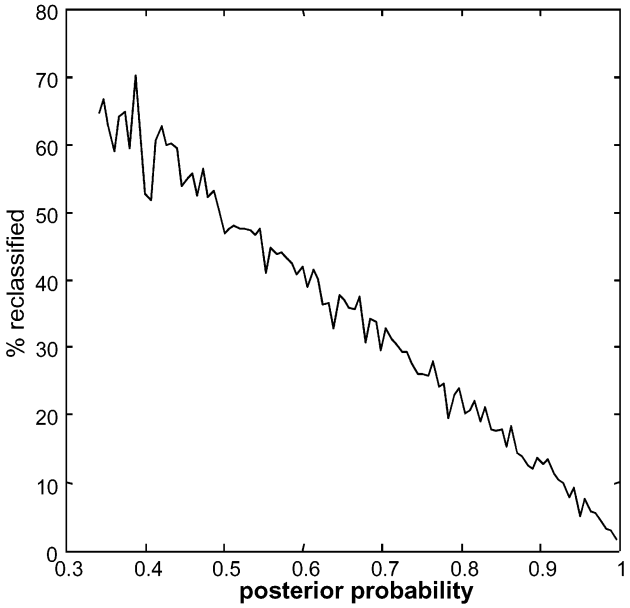

Figure 6. The percent of pixels reclassified during contextual refinement ($\beta = 1.5$) of the 3-component Poisson images as a function of the posterior probability for the initial assignment. Pixels with a very weak probability of belonging to the originally selected class are more likely to be reassigned on the basis of the neighboring pixels.

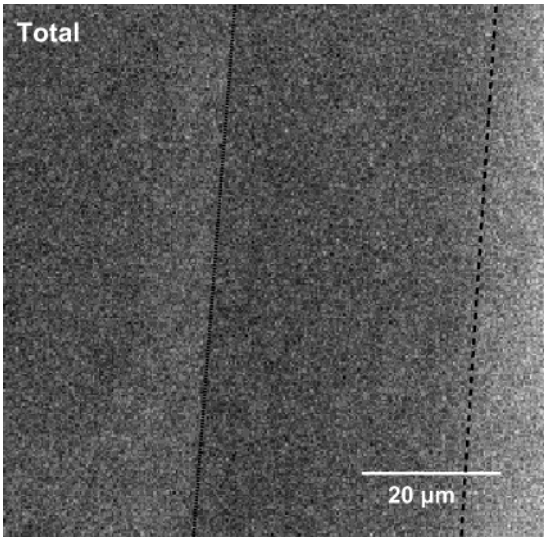

Figure 7. Total ion image from the PNBMA/PIBMA image. Dotted lines show the class boundaries used to calculate the misclassification rates.

Data Analysis. The Poisson and multinomial mixture models were fit from a random sample of 10 000 pixels (of 65 536 possible) for values of K (total chemical classes) from 2 to 6. The estimated pure component spectra, BIC values, and the resulting noncontextual images were examined to aid in the final choice of K. Contextual images were created using the "optimal" choices of K as determined on the basis of the BIC values for both models. Smoothing parameters of $\beta = 0.7$ and 1.5 were used in each case. MATLAB routines were written to perform the analysis and image construction. Each image analysis was completed in a matter of minutes on a personal computer.

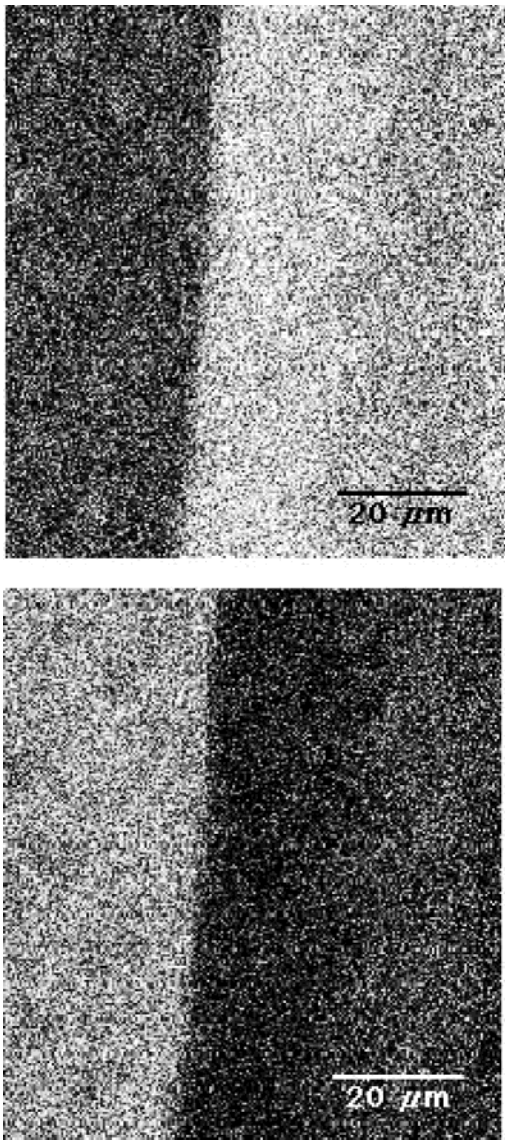

Figure 8. Images of the PNBMA/PIBMA film in which the gray scale corresponds to the posterior probability that each pixel belongs to the class based on the 2-component multinomial model. Black indicates a probability of 1, and white, a probability of 0. The top image shows the posterior probabilities for component 1. Component 2 is displayed in the bottom image.

RESULTS AND DISCUSSION

Figure 1 shows the positive ion spectra for the pure PNBMA and PIBMA. The spectra are highly similar and differ primarily in the ratio of the $C_4H_9^+$ (m/z 57) and $C_4H_7^+$(m/z 55) ions. Figure 2 shows the total ion image as well as single ion images for $C_4H_9^+$ (m/z 57), $C_4H_7^+$(m/z 55), and $C_3H_5^+$(m/z 41). The images reveal some spatial heterogeneity, but it is unclear from these images whether this variation is the result of chemical or topographical differences. The number of chemical phases and their boundaries cannot be readily discerned from the image. Poisson and multinomial mixture models were employed to aid the interpretation.

The Poisson mixture model was fit for values of K between 2 and 6 using random samples of 10 000 pixels. The BIC value was smallest for $K = 3$ and next smallest for $K = 4$. The posterior probabilities for the 3 classes are shown in Figure 3, and the extracted latent profiles are shown in Figure 4. To examine the influence of the smoothing parameter β, images of the 3 component Poisson solution were constructed using $\beta = 0.7$ and $\beta = 1.5$. Figure 5 shows the corresponding segmented images using

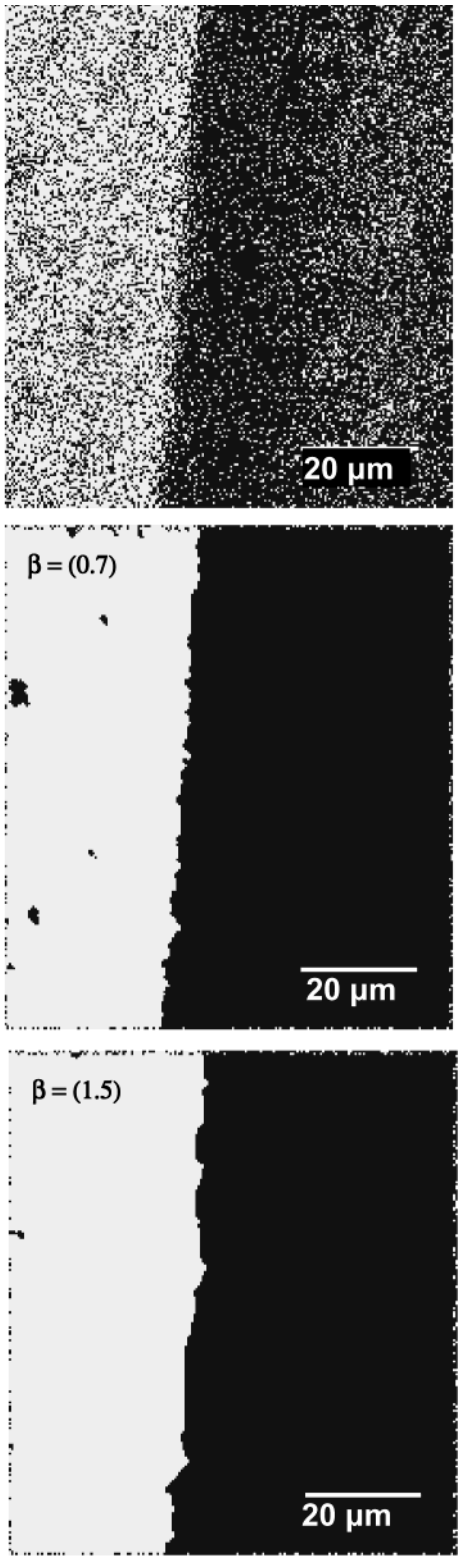

Figure 9. Images generated from the multinomial model by classifying each pixel into one of 2 classes using a smoothing parameter $\beta = 0$ (i.e., no contextual information) (top), $\beta = 0.7$ (middle), and $\beta = 1.5$ (bottom). Pixels assigned to component 1 are shown in white; those assigned to component 2 are shown in black.

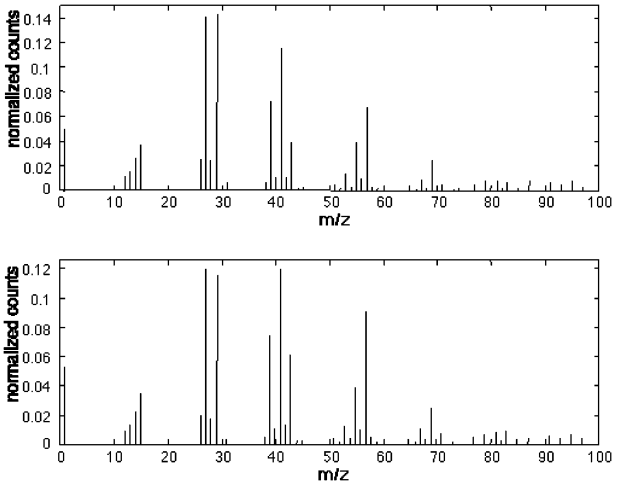

Figure 10. Latent profiles extracted from the PNBMA/PIBMA image using a 2-component multinomial model. The profile for component 1 (corresponding to the white pixels in Figure 9) is shown at the top, and component 2 (Figure 9, black) is shown at the bottom.

the strict posterior probabilities ($\beta = 0$) and contextual refinement with the smoothing parameter $\beta = 0.7$ and 1.5. Class 1 is shown in black, class 2 is shown in gray, and class 3 is shown in white. Contextual refinement significantly reduces the noise in the image. Figure 6 shows the percent of pixels reclassified when using $\beta = 1.5$ as a function of their posterior probability in their original class assignment. It can be observed that reassignment during contextual refinement is most likely when the original assignment was weak.

The latent profiles can be used to assign chemical or physical meaning to the segmented regions. Component 1 (black) constitutes 41.8% of the image area, component 2 (gray) constitutes 15.7% of the image, and component 3 (white) constitutes 42.3% of the image. For the three-component Poisson model, components 1 and 2 (shown in black and gray in Figure 5) have nearly identical peak ratios that correspond well with the pure PIBMA spectra (Figure 1). Both regions are in the PIBMA film. The differences between the two latent profiles are in the total ion intensities rather than in the peak ratios. In component 2 (gray), the average counts per pixel are 1.3 times the average counts per pixel in component 1 (black). Component 2 is an area where the PIBMA film is thicker, and the increased ion intensity can be explained by the corresponding topography. In the latent profile for component 3, the intensity of the mass-41 and mass-57 ions are significantly reduced in comparison to the other components. This region can be identified as PNBMA, and the latent profile compares well with the pure PNBMA spectra.

Misclassification rates were calculated using the class boundaries defined in Figure 7. To reduce error resulting from inaccurate drawing of the boundary, pixels within 2 pixel widths of the class boundaries were ignored. Using the strict Poisson posterior probabilities, 26.7% of the pixels are misclassified. The misclassification rate was significantly reduced using contextual refinement. When using a smoothing factor of 0.7, the misclassification rate was 3.2%, and when using a smoothing factor of 1.5, the misclassification rate was 3.0%. Because components 1 and 2 describe the same chemical component, the misclassification rate was also calculated ignoring misclassifications between components 1 and 2. Using this criteria, the misclassification rate was 21.1% when no smoothing was employed, 2.1% when using $\beta = 0.7$, and 2.0% when using $\beta = 1.5$.

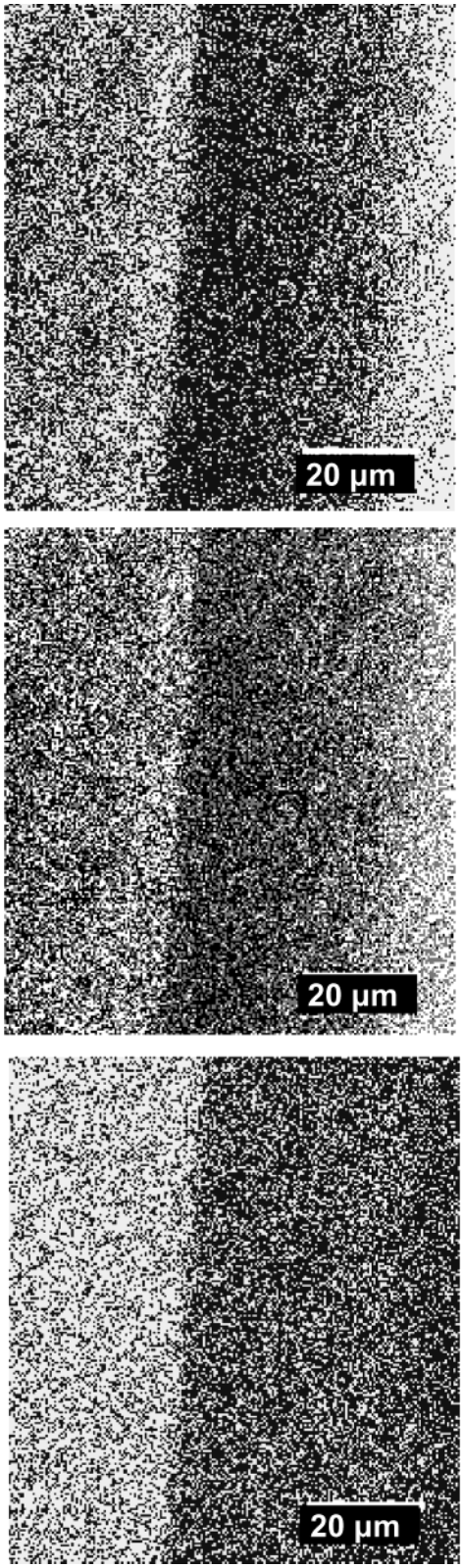

Figure 11. Images generated using a Kohonen neural network. The top and middle images show the results using the raw count data for 2 and 3 classes, respectively. The bottom image shows the results for 2 classes using data normalized to the total ion yield per pixel.

It is worthy of note that, when using the Poisson distribution, the BIC criterion suggests that the 2 component model fits the image worse than either a 3- or 4-component model. The two-component Poisson model does not identify the differences between the two chemical constituents, but instead identifies only the topographical differences. Component 1 encompasses both the white and black regions from the 3-component image (Figure 5), and component 2 separates the higher ion yield region of the PIBMA film (shown in gray in Figure 5).

The multinomial model should correct for higher ion yield areas by conditioning on total ion counts. Using this model, the BIC value was smallest for $K = 2$ and second smallest for $K = 3$. The posterior probabilities for the 2 multinomial components are shown in Figure 8. Figure 9 shows the corresponding segmented images using the strict posterior probabilities ($\beta = 0$) and contextual refinement with the smoothing parameter $\beta = 0.7$ and 1.5. Figure 10 shows the latent profiles extracted from the image for the two components. The first latent profile (top), which corresponds to the white areas in Figure 9, agrees well with both the pure PNBMA spectra and the area identified as PNBMA in the Poisson model. This component constitutes 41.5% of the image area. The second latent profile, constituting 58.5% of the image area, compares well with the pure spectra for PIBMA and encompasses both of the PIBMA regions identified in the Poisson model. As in the Poisson model, contextual refinement significantly reduces the misclassification rate. The misclassification rate is 22.0% when no smoothing is employed, 0.9% when $\beta = 0.7$, and 1.0% when $\beta = 1.5$. When a smoothing parameter β of 1.5 is used, misclassifications occur almost exclusively along the boundary between the two components.

The image was also analyzed with one- and two-dimensional Kohonen neural networks. Because there is much subjectivity in the application of neural networks in the choice of learning rates and neighborhood parameters, we used two methods "off the shelf", that is, that have been recommended for general use. The networks were unable to enhance the contrast between different polymer phases using either 2 or 3 classes. The two components could be visualized if the image was initially normalized to total ion yield but with a misclassification rate of 31.0%, significantly higher than either of the statistically based models. The Kohonen network images are given in Figure 11.

CONCLUSION

This work demonstrates how mixture segmentation models can be adapted for spectral image analysis by suitable choices of probability distributions. The methods developed here show promise for cluster analysis of SIMS images, especially when detected secondary ion counts are very low. The Poisson model can effectively identify features associated with both chemical and topographical effects, whereas the multinomial model is tailored to identify those features associated solely with chemistry. In cases in which the spectra from two chemical components are very similar, contextual refinement can dramatically reduce the misclassification rate. In addition, the latent profiles generated by this statistical process can be comparable to pure components spectra and appear to be of sufficient quality to be used with a spectral library to identify unknown compounds.

Much more work needs to be done to validate the usefulness of these models for routine analysis of SIMS images. We have not analyzed enough variety of images to realize any pitfalls of the methods. More work needs to be done to check the validity of the assumption of Poisson variation of individual peak intensities. Under Poisson variation, the variance of a random variable is equal to its mean. In a study of ion intensities in dynamic SIMS, Adriaens and Adams[13] found that the variations among measurements is greater than that expected under Poisson statistics. This assumption could be incorporated into the mixture models using quasilikelihood methods;[5] however, it is unclear whether their conclusions hold for static TOF-SIMS imaging. In particular, the results of their study do not necessarily generalize to the very low counts with which we are concerned. A separate study of repeated ion intensity measurements using static SIMS imaging would help us validate our modeling assumptions.

The mixture models described here can be extended in three important directions. First, methods can be developed to identify outlier observations that do not appear to belong to any of the recovered chemical phases. This can be important if the goal is to detect particles or other objects that are too sparse to be recognized as a separate class. Second, mixture models can be adapted for fuzzy clustering,[7] in which pixels are allowed to represent more than one chemical phase. Finally, it would be desirable to separate chemical variation from topographic variation in SIMS images where possible. An examination of when such separation can be achieved and development of separation methods would be very useful. The multinomial model described in this paper can be used to find a crude initial solution. This model produces chemically distinct regions independent of topography. Within a chemically distinct region, topographic maps can be created from total ion counts. Because information is lost with the multinomial methods (resulting in noisier images), more efficient methods are desirable. We are currently exploring Poisson mixture models with an additional mixing variable representing the unobserved (latent) topographic level, with the goal of more efficiently separating chemistry from topography.

We have demonstrated the application of the mixture models to time-of-flight secondary ion mass spectrometry (TOF-SIMS) images, but the results show promise for adapting the method for use with a variety of spectral imaging techniques in which spectral reconstruction is desired. The ability of these methods to identify chemically distinct regions and reconstruct pure component spectra when low signal-to-noise ratio, matrix effects, topography, or uneven illumination confound data interpretation offers promise for many types of spectral imaging.

ACKNOWLEDGMENT

We thank the National ESCA and Surface Analysis Center for Biomedical Problems (NESAC/BIO) for the funding of this research through the National Center for Research Resources (NIH Grant RR-01296) and the Montana State University Image and Chemical Analysis Laboratory.

Received for review February 5, 2002. Accepted July 9, 2002.

AC025561I

(13) Adriaens, A.; Adams, F. *Int. J. Mass Spectrom. Ion Processes* **1991**, *108*, 41.